Chapter 5

Spectroscopic Ellipsometry Study of Organic-Inorganic Halide: $FAPbI_xBr_{3-x}$ Perovskite Thin Films by Two-Step Method

Hajime Shirai

Additional information is available at the end of the chapter

http://dx.doi.org/10.5772/intechopen.70281

Abstract

Spectroscopic ellipsometry (SE) was used to investigate the role of isopropyl alcohol (IPA) solvent in the synthesis of organic-lead-halide perovskite $CH(NH_2)_2PbI_xBr_{3-x}$ [$FAPbI_xBr_{3-x}$] thin films including the effect of I/Br composition ratio by the two-step reaction of an amorphous (a-)PbI_xBr_{2-x} layer and FAI_xBr_{1-x} solution diluted in IPA. An optical dispersion model was developed to extract the complex refractive index N (=n + ik), optical transition, and film thickness of $FAPbI_xBr_{3-x}$ perovskites by SE analysis at different I/Br composition ratio as a function of immersion time in a solution of FAI_xBr_{1-x} diluted in IPA. SE combined with X-ray diffraction (XRD), Fourier-transform infrared spectroscopy (FTIR), and scanning electron microscopy (SEM) revealed that Br incorporation into films promoted the densification of $FAPbI_xBr_{3-x}$ perovskite network along with increased film thickness and volume fraction of void. IPA promoted film crystallization of a-PbI_xBr_{2-x} accompanied by the formation of surface roughness, grain boundaries, and voids, followed by enhanced diffusion of FAI_xBr_{1-x} into the grain boundaries/voids in the mesoporous crystallized PbI_xBr_{2-x} network. These processes contribute synergistically to the growth of the perovskite structure.

Keywords: ellipsometry, organic-lead-halide perovskite, two-step reaction, role of isopropyl alcohol (IPA) solvent, growth mechanism

1. Introduction

In recent years, organic-inorganic halide perovskite solar cells have significantly attracted much interest as high-efficiency solar cell material due to their high absorption coefficient, ambipolar carrier transport, and long-carrier diffusion lengths, which have resulted in power conversion efficiencies (PCEs) as high as 20.1% [1–3]. Methylammonium [$(CH_3NH_3)^+$; MA] lead triiodide ($MAPbI_3$), which is used in the most efficient perovskite solar cells, has a bandgap (E_g) of around 1.57 eV [4, 5], a very sharp absorption edge [6], and an impressively

low difference between the open-circuit voltage (V_{oc}) and its bandgap potential (E_g/q) [6–8]. However, the instability of $MAPbI_3$ with respect to humidity, temperature, and light soaking is a serious problem hindering long-term reliability of the photovoltaic performance. Therefore, the formamidinium [$(NH_2)_2CH^+$; FA] lead triiodine ($FAPbI_3$) perovskite, where the ionic radius of the A-site FA^+ ion (253 pm) is larger than that of MA^+ (217 pm), has recently been extensively studied due to better-phase stabilization and higher photovoltaic performance over other systems such as $MAPbI_3$, and better stability for air storage with an extension of the optical absorption edge to the infrared region up to around 840 nm [5]. More recently, interest has extended to the $FAPbI_xBr_{3-x}$ and $Cs_{0.2}FA_{0.8}PbI_xBr_{3-x}$ perovskite, which has even higher stability against humidity as well as temperature. A bandgap is also tunable from 1.43 to 2.35 eV by substitutional doping of bromide ions to iodine sites [9].

In addition, various methods for the fabrication of perovskite thin films have been extensively studied, such as a one-step solution process [10], sequential two-step reaction [11, 12], and vacuum deposition [13]. Although an efficient PCE of around 20% has been achieved using uniform and dense perovskite layers prepared by a one-step solution process [14, 15], this involves complex procedures such as precise control of the composition ratio in the precursor solution and the rate of evaporation to adjust the composition ratio of the perovskite film. An alternative approach is a two-step deposition method using porous PbX_2 (X = I, Cl, Br) films and organic halide solutions such as MAX and FAX diluted in 2-isopropanol alcohol [IPA; $(CH_3)_2COH$] solvent on an electron transport layer such as mesoporous TiO_2 or ZnO, which results in better coverage and uniformity than the one-step process. However, the film morphology of the porous PbX_2 in the two-step deposition method has a strong effect on the chemical reactivity with the alkyl amine halide, which in turn determines the film homogeneity and crystallinity of the resultant perovskite thin films. To control the morphology of PbX_2 films, solvent vapor treatment [16], and additives such as hydriodic acid [17], dimethyl sulfoxide (DMSO), and *N*-methyl-2-pyrrolidone [18] have been tested. For example, Miyadera et al. reported that the rate of perovskite formation from polycrystalline PbI_2 on mesoporous TiO_2 was approximately one order of magnitude faster than that of well-oriented dense PbI_2 on glass [19]. In addition, the type of solvent is sensitive to the morphology of PbI_2. *N*,*N*-Dimethylformamide (DMF; CH_3NCHO) is generally used to promote the crystallization of PbI_2. The use of DMSO or cumene hydroperoxide (CHP; $C_6H_5C(CH_3)_2OOH$), which has lower vapor pressures than DMF, has been reported to suppress the rapid crystallization and to form an amorphous structure that reacts preferentially with MAI diluted in IPA solvent, resulting in a slower rate of crystallization of $MAPbI_3$ and a more homogeneous film structure [20, 21]. However, the role of the polar IPA solvent in the synthesis of $FAPbI_xBr_{3-x}$ perovskites is still not clear because the reaction rate is very fast. Thus, to understand the effect of Br incorporation on the fine structure and the growth mechanism of perovskites by a two-step method from PbI_xBr_{2-x} film and FAI_xBr_{1-x} solution diluted in IPA solvent, a slower reaction rate is preferable from amorphous (a-)PbI_xBr_{2-x} rather than from mesoporous crystalline PbX_2 by immersion in FAX/IPA solution at lower temperatures.

In this chapter, we present the role of the IPA solvent in the synthesis of $FAPbI_xBr_{3-x}$ perovskites including the effect of Br incorporation in the films by a two-step solution process using spectroscopic ellipsometry (SE) as well as X-ray diffraction (XRD), Fourier-transform infrared spectroscopy (FTIR), and scanning electron microscopy (SEM) observation.

http://dx.doi.org/10.5772/intechopen.70281

2. Experimental section

A-PbI_xBr_{2-x} thin films with a film thickness of around 150 nm were prepared on glass by spin coating a mixture of FAI_xBr_{1-x} and PbI_xBr_{2-x} powder (PbI_2:$PbBr_2$ = 3:1 and 3:2 molar ratio) in a DMF/CHP (95:5, v/v) cosolvent at 3000 rpm for 30 s. A-PbI_xBr_{2-x} films prepared using the DMF/CHP cosolvent promoted the growth of perovskite structure after immersion in FAI_xBr_{1-x}/IPA solution, whereas no reaction to form the perovskite occurred in a-PbI_xBr_{2-x} films prepared from 100 vol% DFM solvent. Thus, a-PbI_xBr_{2-x} fabricated with DMF/CHP cosolvent was used as a precursor to promote the formation of perovskite structure. A-PbI_xBr_{2-x} films were immersed in a solution of FAI_xBr_{1-x} (FAI:FABr = 3:1 molar ratio) in IPA solvent for various times (t_{im}) at 25°C. Finally, the $FAPbI_xBr_{3-x}$ films were rinsed with IPA to remove the residual solution and contaminants from the film surface.

The refractive index n and extinction coefficient k of the corresponding $FAPbI_xBr_{3-x}$ films were determined using a phase-modulated spectroscopic ellipsometer (UVISEL, Horiba Jobin Yvon). The ellipsometric angles, Ψ and Δ, which determine the complex reflection coefficient ratio, $\rho = \tan\Psi e^{i\Delta}$, were also measured for 71 points in the range of 1.5–5.0 eV (0.05 eV step) with an integration time of 200 ms at each photon energy. The angle of incidence, θ_i, of the probe light was 70°. The measured values for the n and k spectra, denoted by <n> and <k>, include information regarding the surface roughness, voids, and bulk inhomogeneity of the perovskite film and the PbI_xBr_{2-x} precursor. The bulk component of optical constants for the perovskite films, n and k, and the volume fractions of perovskite and voids (f_{perov}, f_{void}) were determined using a modified amorphous model based on the Forouhi-Bloomer (FB) model described in Eq. (1), combined with the Bruggeman effective medium approximation (EMA) [22, 23]:

$$n(\omega) = \frac{B \cdot (\omega - \omega_j) + C}{(\omega - \omega_j)^2 + \Gamma_j^2} \tag{1}$$

$$k(\omega) = \begin{cases} \dfrac{A_j \cdot E_0 \cdot (\omega - \omega_g)^2}{(\omega - \omega_g)^2 + \Gamma^2} & for\ \omega > \omega_g \\ 0 & for\ \omega > \omega_g \end{cases} \tag{2}$$

where

$$\begin{aligned} B &= \frac{A_j}{\Gamma_j} \cdot [\Gamma_j^2 - (\omega_j - \omega_g)^2] \\ C &= 2 \cdot A_j \cdot \Gamma_j \cdot (\omega_j - \omega_g) \end{aligned} \tag{3}$$

The quantities A_j, Γ_0, ω_j, and ω_g represent the resonance amplitude, the oscillator-broadening parameter, the resonance energy, and the Tauc optical gap, respectively. Spectral fitting was performed using the optical constant for bulk $FAPbI_xBr_{3-x}$ perovskite described in Eq. (1), and f_{perov}, f_{void}, and each film thickness d_i (i = 1, 2, 3), as variables. A probable structure was determined using the optical model by minimization of the standard deviation χ^2 between

the measured and calculated ellipsometric error parameters using a linear regression method as follows [24]:

$$\chi^2 = \frac{1}{2N-M}\sum_{i=1}^{N}\left[\left(\tan\Psi_i^c - \tan\Psi_i^m\right)^2 - \left(\cos\Delta_i^c - \cos\Delta_i^m\right)^2\right] \quad (4)$$

where the superscripts *c* and *m* represent the calculated and measured values, and *N* and *M* are the numbers of the measured and calculated wavelengths, respectively.

The fine structures of the a-PbI_xBr_{2-x} and perovskite $FAPbI_xBr_{3-x}$ thin films were also evaluated using X-ray diffraction (Bruker D8 ADVANCE ECO) with the diffractometer in Bragg-Brentano mode using Cu Kα radiation with a Lynxeye XE detector, Fourier-transform infrared spectroscopy (Shimadzu spectrometer, IRTracer-100), field emission scanning electron microscopy (FESEM; S4800, Hitachi High Technologies, Japan) with energy-dispersive X-ray spectroscopy (EDX) (Bruker XFlash 5030/Quantax 400), and atomic force microscopy (AFM; NanonavieII/SPI-3800, Hitachi High-Tech Science, Japan) to support the results of the SE analysis.

3. Results and discussion

3.1. Characterization of $FAPbI_xBr_{3-x}$ perovskite films

Figure 1a shows XRD patterns of corresponding $FAPbI_xBr_{3-x}$ films on glass synthesized by the two-step method using a-PbI_xBr_{2-x} layer and FAI_xBr_{1-x} solution in IPA at various t_{im}. No XRD diffraction peaks that would indicate a crystalline phase were observed for spin-coated

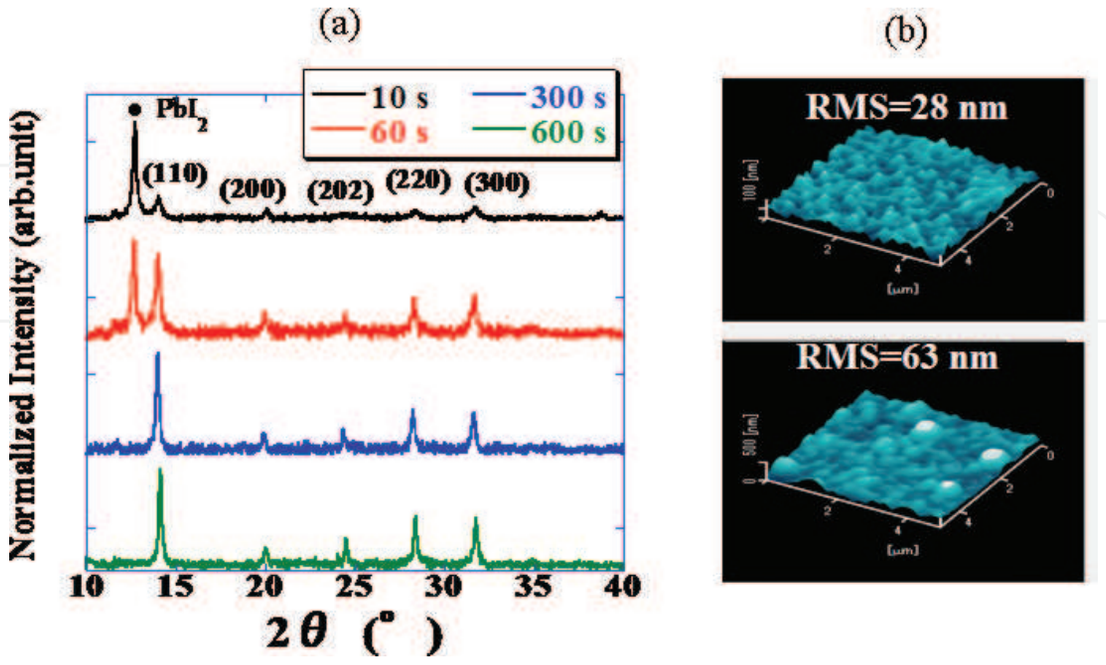

Figure 1. (a) XRD pattern of $FAPbI_xBr_{3-x}$ films synthesized at various t_{im}. (b) AFM image of t_{im} of 10- and 600-s-immersed films.

http://dx.doi.org/10.5772/intechopen.70281

PbI_xBr_{2-x}, which suggests that the film structure was mainly amorphous. However, the film immersed for 10 s showed a diffraction peak at 2θ = 12.6°, which is attributed to the (1 0 0) crystal orientation in PbI_xBr_{2-x}, and peaks were observed at 2θ =14.6° and 28°, which correspond to the (1 1 0) and (2 2 0) diffraction peaks of the $FAPbI_xBr_{3-x}$ perovskites, respectively. A trace of the hexagonal structure δ phase was also indicated by the peak at 2θ = 11.7°, which is undesirable with regard to the photovoltaic performance. The diffraction peaks attributed to the $FAPbI_xBr_{3-x}$ perovskites increased with suppression of the δ phase peaks and the diffraction peak at 2θ =12.6° attributed to the (1 0 0) crystal orientation in PbI_xBr_{2-x} when t_{im} was increased up to 600 s. The AFM image of 10 and 600 s immersed film is also shown in **Figure 1b**. RMS is increased from 28 to 63 nm. These results suggest that the I/Br composition ratio determines the fine structure, and the formation of a perovskite structure is promoted together with an increase of the surface roughness, grain boundaries, and voids.

3.2. SE study of perovskite $FAPbI_xBr_{3-x}$ films

Figure 2 shows <*n*> and <*k*> spectra for the $FAPbI_xBr_{3-x}$ perovskite films prepared at various t_{im}, including those for the a-PbI_xBr_{2-x} precursor film. Once the a-PbI_xBr_{2-x} layers were immersed in the FAI_xBr_{1-x} solution in IPA, the <*n*> value decreased gradually, which suggests an increase in porosity, voids, and/or surface roughness in the a-PbI_xBr_{2-x} structure. By contrast, the <*k*> value that corresponds to optical absorption $\alpha = 4\pi k/\lambda$ ($\alpha = 4\pi k/\lambda$) in the visible to near-infrared region was markedly increased for the film immersed for 10 s, followed by a decrease with t_{im} up to 600 s. Thus, the time evolutions of <*n*> and <*k*> spectra with t_{im} include information of the growth chemistry of the $FAPbI_xBr_{3-x}$ perovskite structure by the two-step process of a-PbI_xBr_{2-x} layer formation and immersion in the FAI_xBr_{1-x} solution in IPA.

Figure 3a shows the <*n*> and <*k*> spectra for the spin-coated a-PbI_xBr_{2-x} layer included in **Figure 2** together with the best-fit calculated spectra. A single-layer model consisting of a modified FB model was used to determine the optical constant of the bulk component of the a-PbI_xBr_{2-x} layer and the film thickness. The best-fit <*n*> and <*k*> spectra are also included as dotted lines. Good-fitting results were obtained over the entire energy region from 1.5 to 5 eV

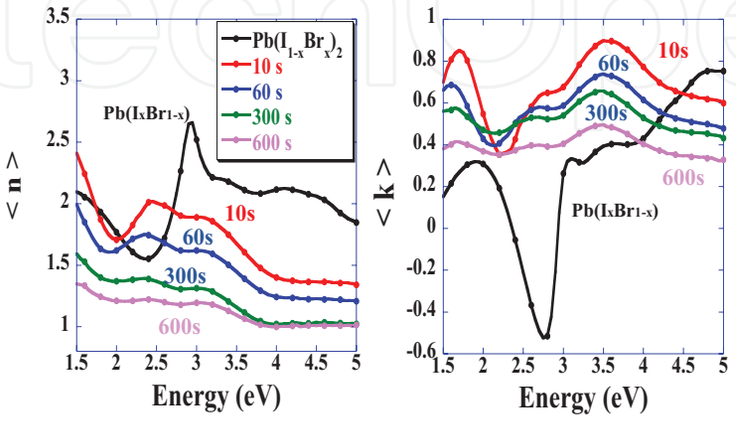

Figure 2. Measured <*n*> and <*k*> spectra for $FAPbI_xBr_{3-x}$ perovskite films prepared on glass by the immersion of a-PbI_xBr_{2-x} in a solution of FAI_xBr_{1-x} in IPA solvent at various t_{im}.

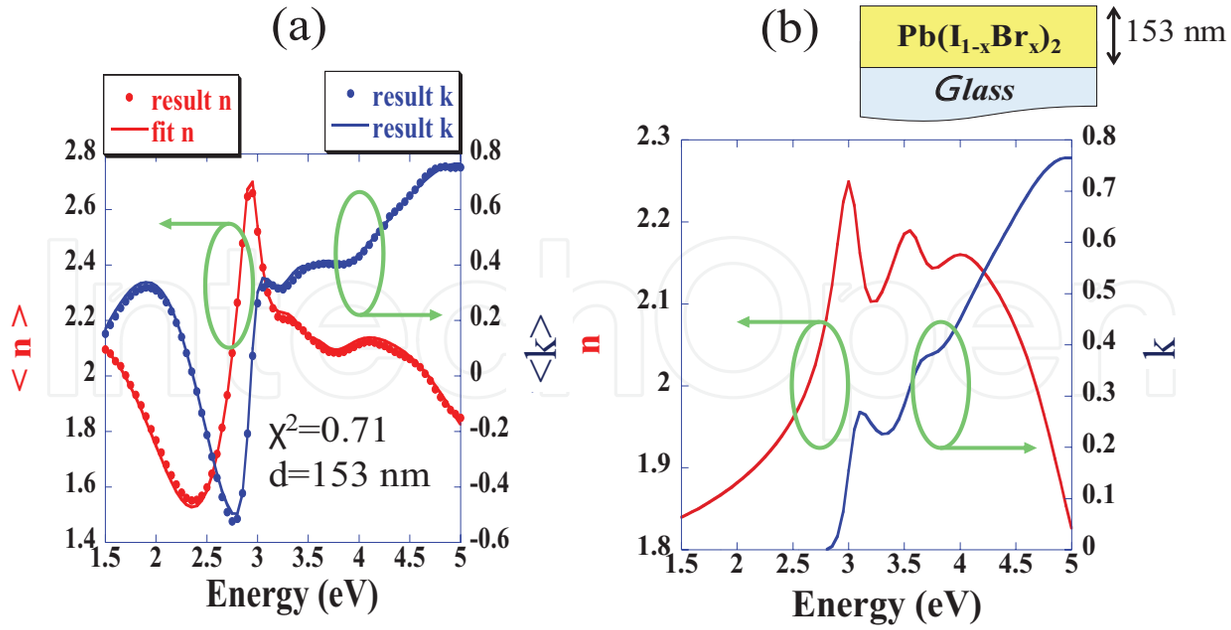

Figure 3. (a) Measured <*n*> and <*k*> spectra for spin-coated a-PbI_xBr_{2-x} included in **Figure 2** together with the best-fit calculated spectra. (b) The *n* and *k* spectra for bulk component of a-PbI_xBr_{2-x} extracted by a spectral-fitting procedure using a single-layer model.

with χ^2 of 0.71. The *n* and *k* spectra of the a-PbI_xBr_{2-x} bulk component along with the optical model used for the spectra fitting are shown in **Figure 3b**. The film thickness was 153 nm, which was almost consistent with that determined by FESEM observation and a thickness profiler. The fine structures were observed at 3.1, 3.7, and 4.2 eV in a-PbI_xBr_{2-x}, which are analogous to those at 2.95, 3.50, and 3.9 eV attributed to the respective $\Gamma_4^+ \rightarrow \Gamma_4^-(p_{xy})$, $\Gamma_4^+ \rightarrow \Gamma_4^-(p_z)$, and $A_4^+ \rightarrow A_4^-$ (conduction band) optical band transitions in PbI_2 [25]. These high-energy shifts in the fine structures are due to the addition of Br.

To understand the formation mechanism of perovskite structure using a two-step method, the measured <*n*> and <*k*> spectra were analyzed using two- or three-layer models consisting of a perovskite $FAPbI_xBr_{3-x}$ top layer and a PbI_xBr_{2-x} underneath layer using constant (*n*, *k*) spectra for $FAPbI_xBr_{3-x}$ and PbI_xBr_{2-x}, and f_{perov}, $f_{Pb(I,Br)2}$, f_{void}, and d_i as variables. However, the (*n*, *k*) spectra calculated using several optical models deviated far from the measured spectra, which suggests that modelization of the optical constant for the transitional stage from a-PbI_xBr_{2-x} to the $FAPbI_xBr_{3-x}$ perovskite structure should be considered at each t_{im}. Among single-layer to four-layer optical models, the three-layer model showed the best fit with four Lorentzian oscillators for a PbI_xBr_{2-x} and $FAPbI_xBr_{3-x}$ composite phase including f_{perov}, f_{void}, and d_i (i = 1, 2, 3) as variables.

Figure 4a shows the best-fit *n* and *k* spectra for the $FAPbI_xBr_{3-x}$ perovskite bulk component prepared at various t_{im}. The *n* value increased in the first 10 s and then decreased with increasing t_{im}, whereas the *k* values increased with the appearance of several fine structures attributed to the optical band transition of $FAPbI_xBr_{3-x}$. The absorption edge shifted to a lower energy from 3.1 to 1.63 eV for 60-s immersion and then became almost independent of t_{im}. In

http://dx.doi.org/10.5772/intechopen.70281

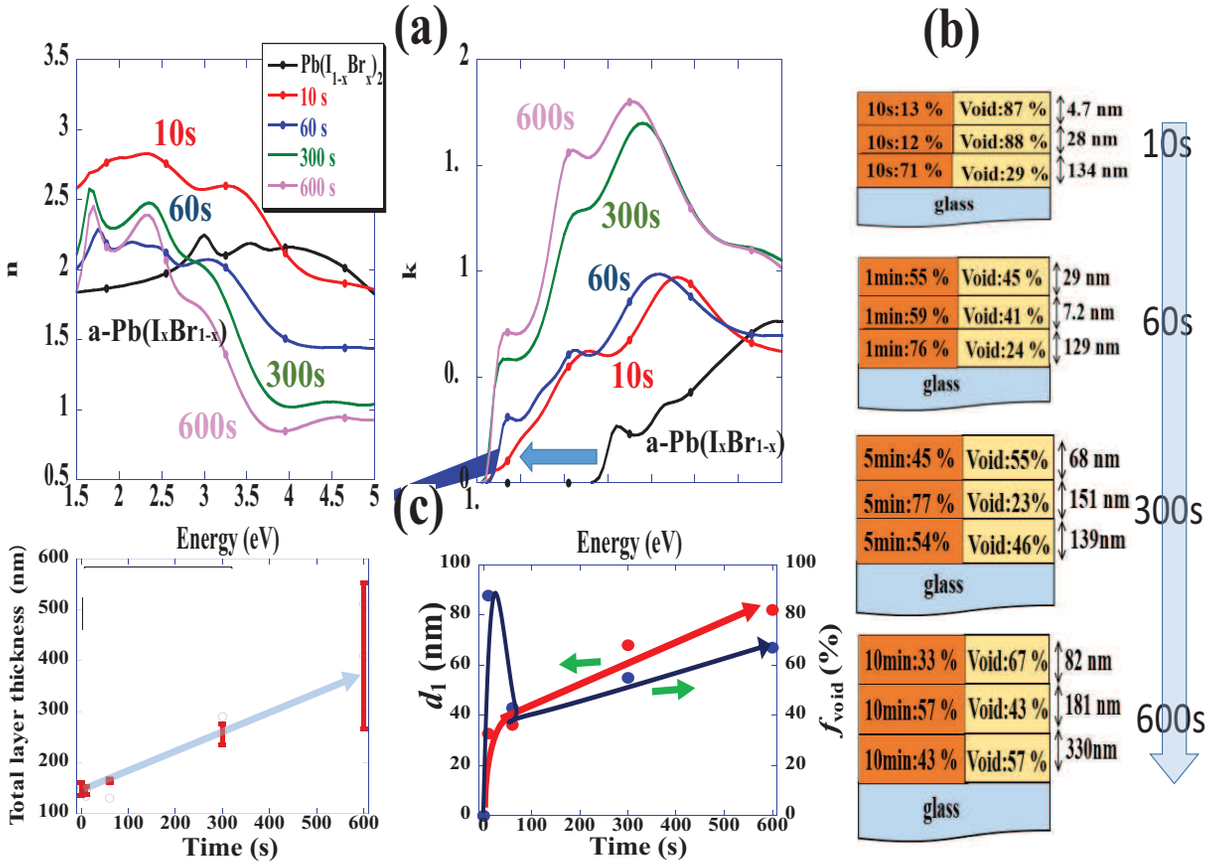

Figure 4. (a) Best-fit n and k spectra for the $FAPbI_xBr_{3-x}$ perovskite bulk component for corresponding films prepared at various t_{im}. (b) Best-fit optical models for corresponding films at various t_{im}. (c) Total film thickness d, d_1, and f_{void} in the top layer plotted as a function of t_{im}.

addition, fine structures at 2.55 and 3.8 eV were shifted to the infrared region with an increase in their amplitude when t_{im} was increased up to 600 s. In particular, the layer immersed for 600 s exhibited four fine structures in the k spectra at 1.63, 2.52, 3.25, and 4.79 eV, which were attributed to the optical transition of the perovskite structure.

The best-fit optical models for the various t_{im} are summarized in **Figure 4b**, including the corresponding χ^2 values. For the a-PbI_xBr_{2-x} films immersed for 10 and 60 s, no significant differences in f_{perov} and f_{void} were observed between the two- and three-layer models. The f_{perov} and f_{void} values were almost identical for both the top and intermediate layers, despite the use of the three-layer model. A prominent feature was that f_{void} was increased significantly for the entire film thickness, despite being immersed for only 10 s, which suggests that the rate of crystallization of a-PbI_xBr_{2-x} was much quicker than the rate of formation of the perovskite structure. The diffusion of FAI_xBr_{1-x} into the voids and/or grain boundaries resulted in the simultaneous formation of large amounts of free volume and an increase in the film thickness, resulting in a decrease in the refractive index (**Figure 4a**). The best-fit d ($=d_1 + d_2 + d_3$), d_1, and f_{void} for the top layer are summarized as a function of t_{im} in **Figure 5c**, together with those determined using a thickness profiler. The value of d increased from 150 nm for a-PbI_xBr_{2-x}

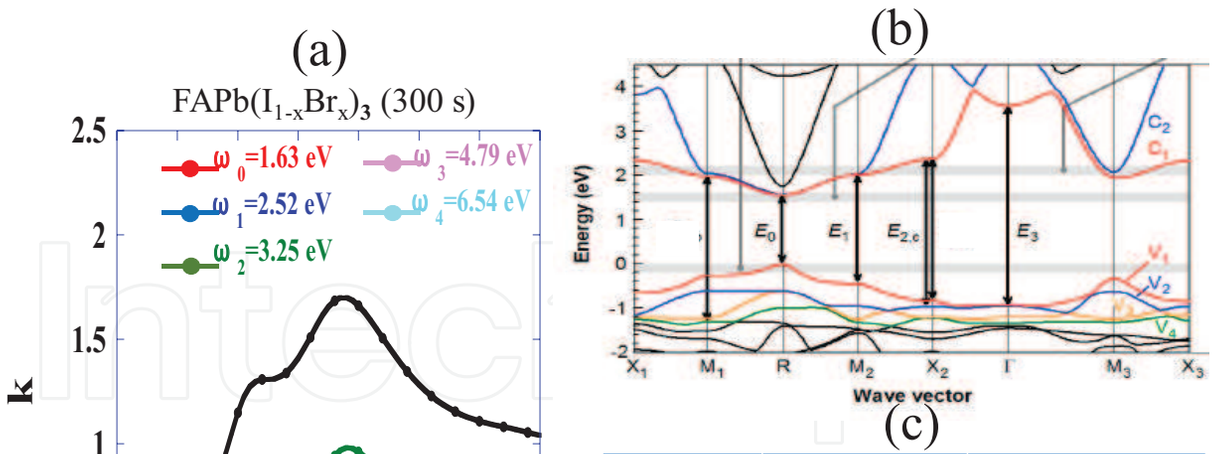

(c)

Optical transition	$MAPbI_3$	$FAPb(I_{1-x}Br_x)_3$
ω_0	1.61 (eV)	1.63 (eV)
ω_1	2.53 (eV)	2.52 (eV)
ω_2	3.24 (eV)	3.25 (eV)
ω_3	4.4 (eV)	4.79 (eV)
	7.29 (eV)	6.54 (eV)

Figure 5. (a) *k* spectrum for the $FAPbI_xBr_{3-x}$ perovskite immersed in a solution of FAI_xBr_{1-x} in IPA solvent for 600 s, including each optical transition component obtained by the spectral-fitting procedure. (b) Band structure of the $MAPbI_3$ perovskite determined from DFT calculations [26]. (c) Comparison of the optical transition components between $MAPbI_3$ [26] and $FAPbI_xBr_{3-x}$ perovskite.

to 350 nm for the $FAPbI_xBr_{3-x}$ perovskites. The volume fraction of voids and the thickness of f_{void} and d_1 corresponding to the top layer increased significantly during the initial 10–60 s of immersion, after which they increased only gradually with t_{im}. These results imply that the formation of the perovskite structure proceeds with the formation of free space within the PbI_xBr_{2-x} network due to the insertion of the organic FA cation.

Figure 5a shows the *n* and *k* spectra for the $FAPbI_xBr_{3-x}$ perovskite bulk component after immersion for 600 s, including each of the optical transition components determined by the deconvolution method. The electronic structure of $MAPbI_3$ determined from DFT calculations was reported by Shirayama et al. [26] (**Figure 5b**). The comparison between optical transition energies for ω_0, ω_1, ω_2, and ω_3 of $MAPbI_3$ and $FAPbI_xBr_{3-x}$ is summarized in **Figure 5c** [26, 27]. Similar to the band structure of $MAPbI_3$, four distinct optical transitions in $FAPb(I_xBr_{1-x})_3$ were observed at 1.63, 2.52, 3.25, and 4.79 eV, which may be attributed to direct semiconductor-type transitions at the R, M, X, and Γ points in the pseudo-cubic Brillouin zone, respectively. According to Shirayama et al., a sharp optical transition at 3.25 eV in PbI_xBr_{1-x} is probably excitonic, and the transition energy of this peak is close to that of the peak for $MAPbI_3$. The absorption peak at 3.1 eV in a-PbI_xBr_{2-x} is relatively sharp, while the corresponding peak was broad for PbI_xBr_{2-x} after immersion for 10 s. Two distinct optical transitions at 1.77 and 2.5 eV were observed for the film immersed for 60 s. Here, the absorption peak at 2.5 eV is probably attributed to a layered structure of PbI_xBr_{2-x} analogous to that of PbI_2 reported elsewhere [28].

http://dx.doi.org/10.5772/intechopen.70281

The onset of the optical transition (ω_0) was shifted to 1.75 eV and was almost independent of the immersion time over 300 s.

Figure 6 shows the changes of the optical transition energies, ω_0, ω_1, ω_2, and ω_3 with t_{im}. The optical transition energies ω_0, ω_1, and ω_2 shift to the infrared region and their amplitude increases when t_{im} was increased up to 600 s. Among the four optical transitions, the lower-energy shift of the ω_2 component from 3.85 to 3.4 eV was prominent and attributed to the 6*s*-6*p* transition of Pb^{2+}. Hirasawa et al. reported the exciton features in zero- (0D), two- (2D), and three-dimensional (3D) networks of $[PbI_6]^{4-}$ octahedra in $MA_4PbI_6{\cdot}2H_2O$, $(C_{10}H_{21}NH_3)_2PbI_2$, and $MAPbI_3$ from reflection spectra measured at 4 K [29]. The energy of the lowest exciton decreases significantly as the dimension is increased and was 3.4, 2.55, and 1.633 eV for the 0D, 2D, and 3D network compounds, respectively. These results make an analogy that the process for the formation of the $FAPbI_xBr_{3-x}$ perovskite from a-PbI_xBr_{2-x} is attributed to a decrease in the dimension of the crystal structure based on $[Pb(IBr)_6]^{4-}$.

3.3. Effect of *x* on the fine structure of $FAPbI_xBr_{3-x}$ perovskite films

Figure 7 shows measured I_s (=sin2ψsinΔ) and I_c (=sin2ψcosΔ) spectra for $FAPbI_xBr_{3-x}$ perovskite films with two different PbI_2:$PbBr_2$ molar ratios of 3:1 and 3:2, including the best-fitted calculated spectra using the optical model shown on the right. The *n* of an I:Br = 3:2 film was larger than that of 3:1 film with increased film thickness and f_{void}. Thus, increased Br incorporation into $FAPbI_3$ promoted the densification of perovskite network, resulting in the increased film thickness and f_{void}, as far as a two-step method with immersion to FAIBr/IPA solution was

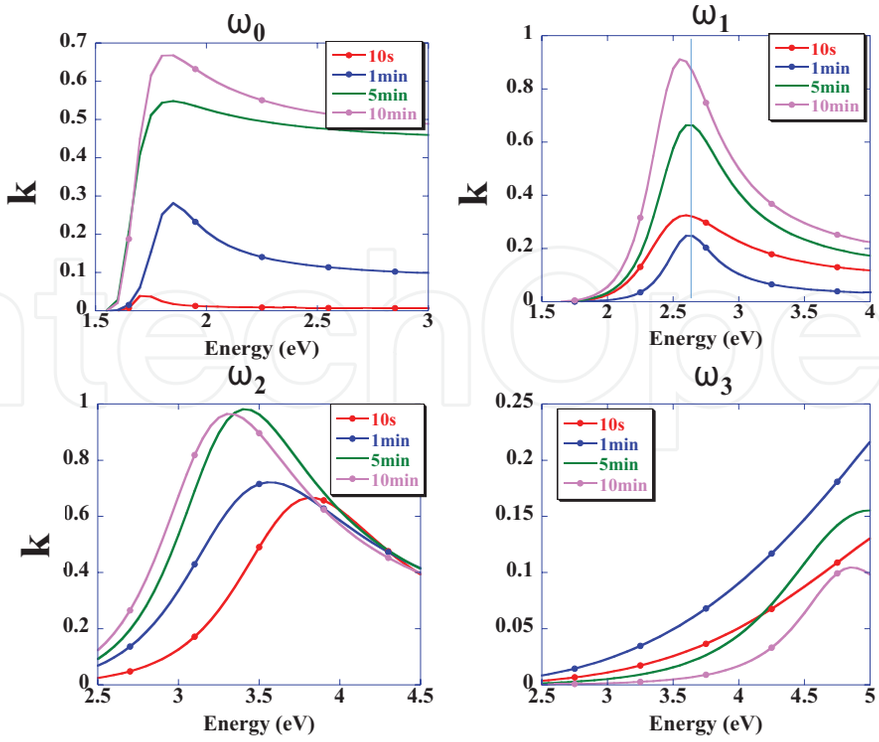

Figure 6. Changes of optical transition for ω_0, ω_1, ω_2, and ω_3 of PbI_xBr_{2-x} immersed in FAI_xBr_{1-x}/IPA solution at various t_{im}. Each optical transition component was determined by the spectral-fitting procedure.

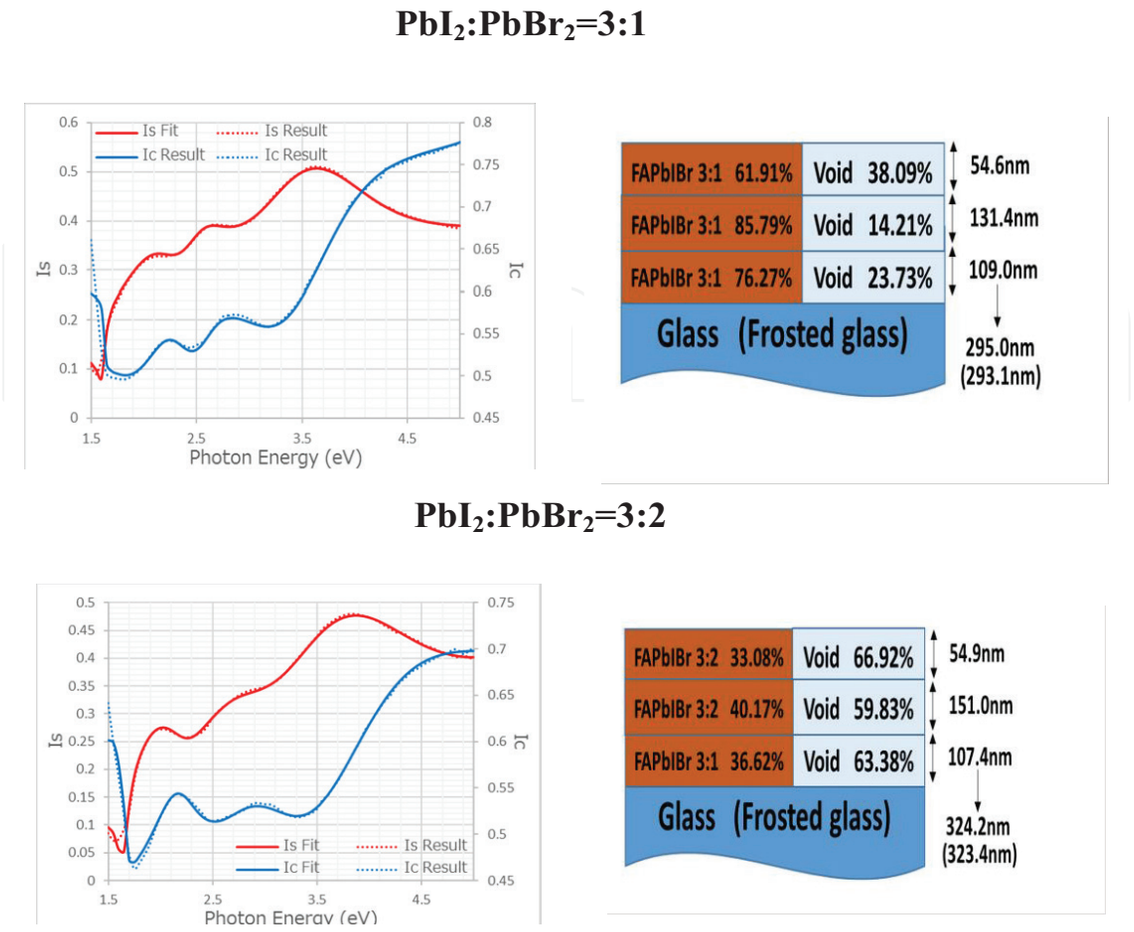

Figure 7. Measured I_s and I_c spectra of $FAPbI_xBr_{3-x}$ perovskite films with PbI_2:$PbBr_2$ = 3:1 and 3:2 molar ratio including the best-fitted calculated spectra. Corresponding best-fitted optical model.

used. In fact, XRD pattern and PL revealed that lattice parameter decreased with higher-edge emission peak energy when Br composition was increased. SE also showed an increase of the refractive index for $FAPbI_xBr_{3-x}$ perovskite phase together with an increase of the film thickness and volume fraction of void. In fact, RMS increased from 39 nm for 3:1 to 46 nm for 3:2 films in the 20 × 20-μm^2 area. These findings imply that Br incorporation into $FAPbI_xBr_{3-x}$ perovskite films promotes the densification of perovskite network, resulting in the increase in the free volume as a void and film thickness. In addition, prominent sub-gap absorption tail in the 3:2 film compared to that of 3:1 film suggests that the defect originates from the increased grain boundary of $FAPbI_xBr_{3-x}$ (3:2) perovskite phase for larger Br composition ratio.

3.4. Role of IPA solvent in the synthesis of $FAPbI_xBr_{3-x}$ perovskites

Figure 8a and **b** shows XRD pattern and FTIR spectra of a-PbI_xBr_{2-x} film before and after immersion into IPA solvent alone for 10 s. The inset of **Figure 8a** also shows AFM images of the corresponding PbI_xBr_{2-x} films. Despite immersion for only 10 s, the peak at 2θ = 12.7° attributed to the crystalline PbI_xBr_{2-x} (1 0 0) diffraction was observed, which suggests that the crystallization

http://dx.doi.org/10.5772/intechopen.70281

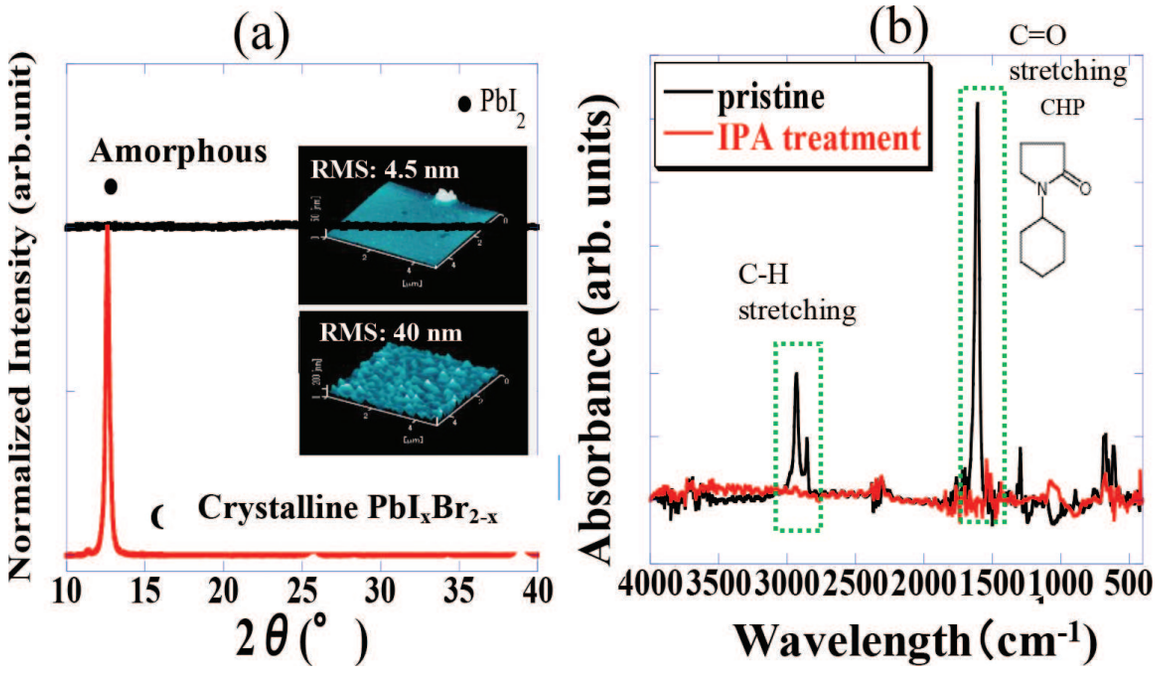

Figure 8. (a) XRD pattern and (b) FTIR spectra of a-PbI_xBr_{2-x} film before and after immersion into IPA solvent alone for 10 s. The inset of **Figure 8a** shows the AFM image of corresponding PbI_xBr_{2-x} before and after immersion into IPA solvent alone without FAI_xBr_{1-x}.

of the film can be attributed mainly to immersion in the IPA solvent. The FTIR spectra also revealed that the removal of the C═O-bending mode and C─H-stretching mode attributed to residual CHP in a-PbI_xBr_{2-x} was promoted by the IPA solvent. Thus, film crystallization of a-PbI_xBr_{2-x} was promoted by the removal of residual CHP in a-PbI_xBr_{2-x} and was accompanied by the formation of mesoporous crystallized PbI_xBr_{2-x} with large amounts of voids and/or grain boundaries.

Figure 9 shows n and k spectra for a-PbI_xBr_{2-x} before and after immersion into IPA solvent alone for 10 s. The best-fit optical models are shown in the upper panels. A prominent feature was that the n value decreased markedly with a red shift of the absorption edge onset corresponding to film crystallization with an increase in f_{void}. The significant decrease in n is due to crystallization and the destruction of the mesoporous in a-PbI_xBr_{2-x}. These results imply that IPA had a significant effect to promote crystallization of the a-PbI_xBr_{2-x} film with an associated decrease in the bandgap due to a phase transition from 0D to 3D $[Pb(I_xBr_{1-x})_6]^{4-}$ octahedral clusters. These factors are the main contributors to the formation of the $FAPbI_xBr_{3-x}$ perovskite network. Notable spectral features were the appearance of broad and sharp absorptions at 2.2 (probably due to defects/disorder) and 2.48 eV ($A_4^+ \rightarrow A_4$) assigned as the first exciton region in 2D PbI_xBr_{2-x}, in addition to those at 3.1, 3.5, and 3.9 eV due to film crystallization. In addition, no significant change in the film thickness was observed after immersion into the IPA solvent, but only the formation of voids, which suggests that immersion in IPA did not contribute to an increase of the film thickness.

From these results, the growth mechanism for the formation of $FAPbI_xBr_{3-x}$ perovskites from an a-PbI_xBr_{2-x} layer and FAI_xBr_{1-x}/IPA solution is considered to be as follows (**Figure 10**) [30].

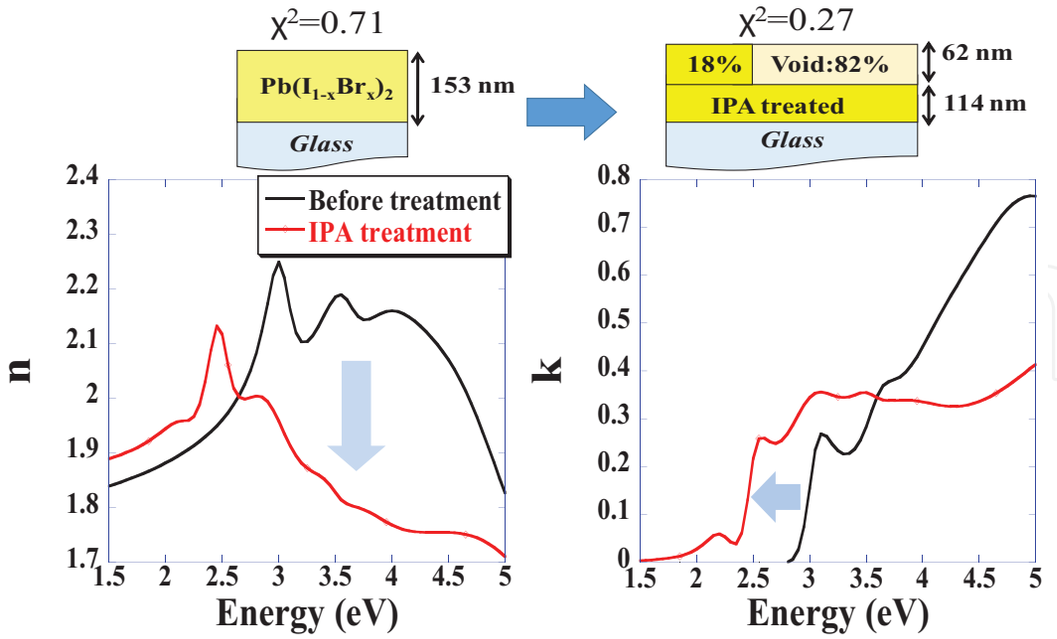

Figure 9. Bulk *n* and *k* spectra component for PbI_xBr_{2-x} films on glass before (black) and after (red) immersion into IPA solvent for 10 s. The best-fit optical model and χ^2 value are shown on the top.

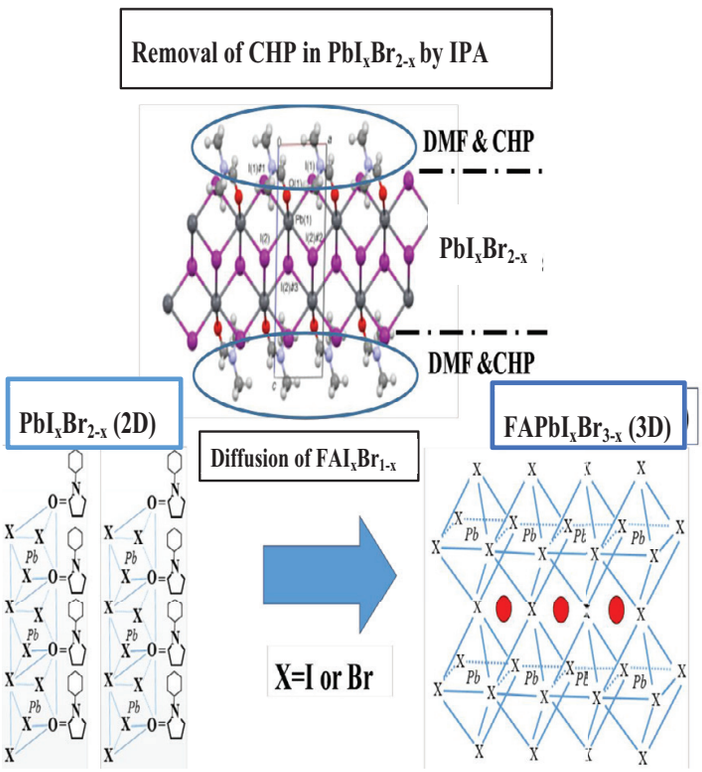

Figure 10. Schematic of the formation mechanism of $FAPbI_xBr_{3-x}$ perovskites from a-PbI_xBr_{2-x} layer and a solution of FAI_xBr_{1-x} in IPA solvent. The formation of the perovskite structure is accompanied by the removal of coordinated CHP in the a-PbI_xBr_{2-x} network during immersion in the IPA solvent.

http://dx.doi.org/10.5772/intechopen.70281

$FAPbI_xBr_{3-x}$ perovskites include an octahedral PbX_6 (X = I, Br) complex with coordinated CHP solvent molecules. When a-PbI_xBr_{2-x} including ─CHP groups is immersed in the IPA solvent, C═O and C─H groups in coordinated CHP are preferentially removed by IPA solvent, which results in the promotion of a-PbI_xBr_{2-x} film crystallization and the formation of a large amount of voids and/or grain boundaries in the network. The diffusion of FAI_xBr_{1-x} into the voids/grain boundaries of the crystalline PbI_xBr_{2-x} phase is simultaneously promoted and leads to the formation of the $FAPbI_xBr_{3-x}$ perovskite structure with an increase in the film thickness. In addition, no XRD diffraction peaks attributed to the perovskite structure were observed for vacuum-evaporated FAI_xBr_{1-x} as a precursor layer without a polar solvent such as IPA and CHP on a-PbI_xBr_{2-x} films, which implies that the IPA solvent promotes the growth of the perovskite structure.

4. Conclusions

1. The effect of Br incorporation into $FAPbI_3$ perovskite films is to promote the densification of perovskite network, resulting in the increase in the free volume as a void and film thickness. In addition, prominent sub-gap absorption tail in the 3:2 film compared to that of 3:1 film suggests that the defect originates from the increased grain boundary of perovskite phase for larger Br compositional ratio.
2. The role of IPA solvent in the synthesis of $FAPbI_xBr_{3-x}$ perovskites from an a-PbI_xBr_{2-x} thin layer and a solution of FAI_xBr_{1-x} in IPA solvent was investigated using SE combined with characterization by XRD and FTIR analysis. IPA played a significant role to promote crystallization of the a-PbI_xBr_{2-x} film through the removal of coordinated CPH from the a-PbI_xBr_{2-x} network, accompanied by the formation of grain boundaries, voids, and surface roughness. The diffusion of FAI_xBr_{1-x} into the voids and/or grain boundaries resulted in the simultaneous formation of large amounts of free volume and an increase in the film thickness, resulting in a decrease in the refractive index. The red shift of absorption edge from 3.4 to 1.73 eV is attributed to a phase transition from 0D to 3D $[PbX_6]^{4-}$ octahedral clusters. These factors are the main contributors to the formation of the $FAPbI_xBr_{3-x}$ perovskite network.

Acknowledgements

The author thanks Dr. Yohei Numata and Professor Tsutomu Miyasaka of Toin Yokohama University for fabrication of the perovskite thin film solar cells.

Author details

Hajime Shirai

Address all correspondence to: shirai@fms.saitama-u.ac.jp

Graduate School of Science and Engineering, Saitama University, Saitama, Japan

References

[1] Kojima A, Terashima K, Miyasaka T, Shirai Y. Novel halide compounds (2). In: 210th ECS Meeting. Pennington, NJ: The Electrochemical Society; 2006. p. 397

[2] Ishii A, Jena AK, Miyasaka T. Fully crystalline perovskite-perylene hybrid photovoltaic cell capable pf 1.2 V output with a minimized voltage loss. APL Materials. 2014;**2**:091102

[3] Green MA, Ho-Ballie A, Snaith HJ. The emergence of perovskite solar cells. Nature Photonics. 2014;**8**:506-514

[4] Kim HS, Lee CR, Im J-H, Lee KB, Moehl T, Marchiro A, Moon SJ, Humphry-Baker R, Yum J-H, Moser JE, Grätzel M, Park NG. Lead iodine perovskite sensitized all-solid state submicron thin film mesoscopic solar cell with efficiency exceeding 9%. Scientific Reports. 2012;**2**:1-7

[5] Eperon GE, Stranks SD, Menelaou C, Johnson MB, Herz LM, Snaith HJ. Formamidinium lead trihalide: A. Broadly tunable perovskite for efficient planer heterojunction solar cells. Energy & Environmental Society. 2014;**7**:982-988

[6] De Wolf S, Holovsky J, Moon SJ, Löper P, Niesen B, Ledlinsky M, Haug FJ, Yum J-H, Ballif C. Organometallic halide perovskites: Sharp optical absorption edge and its relation to photovoltaic performance. Journal of Physical Chemistry Letters. 2014;**5**:1035-1039

[7] Snaith HJ. Perovskites: The emergence of a new era for low-cost, high-efficiency solar cells. Journal of Physical Chemistry Letters. 2013;**4**:3623-3630

[8] Topic M, Geisthardt RM, Sites JR. Performance limits and status of single junction solar cells with emphasis on sigs on CIGS. IEEE Journal of Photovoltaics. 2014;**5**:1-6

[9] Jeon NJ, Noh JH, Yang WS, Kim YC, Ryu S, Seo J, Seok SI. Compositional engineering of perovskite materials for high-performance solar cells. Nature. 2015;**517**:476-480

[10] Kojima A, Teshima K, Shirai Y, Miyasaka T. Organometal halide perovskites as visible-light sensitizers for photovoltaic cells. Journal of the American Chemical Society. 2009;**131**:6050-6051

[11] Burschka J, Pellet N, Moon S-J, Humphry-Baker R, Gao P, Nazeeruddin MK, Grätzel M. Sequential deposition as a route to high-performance perovskite-sensitized solar cells. Nature. 2013;**499**:316-320

[12] Im J-H, Jang I-H, Pellet N, Grätzel M, Park N-G. Growth of $CH_3NH_3PbI_3$ cuboids with controlled size for high-efficiency perovskite solar cells. Nature Nanotechnology. 2014;**9**:927-932

[13] Liu M, Johnston MB, Snaith HJ. Efficient planar heterojunction perovskite solar cells by vapor deposition. Nature. 2013;**501**:395-398

[14] Jeon NJ, Noh JH, Kim YC, Yang WS, Ryu S, Seok SI. Solvent engineering for high-performance inorganic–organic hybrid perovskite solar cells. Nature Materials. 2014;**13**:897-903

[15] Xiao M, Huang F, Huang W, Dkhissi Y, Zhu Y, Etheridge J, Gray-Weale A, Bach U, Cheng Y-B, Spiccia L. A fast deposition-crystallization procedure for highly efficient lead iodide perovskite thin-film solar cells. Angewandte Chemie International Edition. 2014;**53**:9898-9903

[16] Song J, Zheng E, Bian J, Wang X-F, Tian W, Sanehira Y, Miyasaka T. Low-temperature SnO_2-based electron selective contact for efficient and stable perovskite solar cells. Journal of Materials Chemistry. 2015;**A3**:10837-10844

[17] Yang L, Wang J, Leung WW-F. Lead iodide thin film crystallization control for high-performance and stable solution-processed perovskite solar cells. ACS Applied Materials & Interfaces. 2015;**7**:14614-14619

[18] Jo Y, Oh KS, Kim M, Kim K-H, Lee H, Lee C-W, Kim DS. High performance of planar perovskite solar cells produced from PbI_2(DMSO) and PbI_2(NMP) complexes by intramolecular exchange. Advanced Materials Interfaces. 2016;**3**:1-7

[19] Miyadera T, Shibata T, Koganezawa T, Murakami TN, Sugita T, Tanigaki N, Chikamatsu M. Crystallization dynamics of organolead halide perovskite by real-time X-ray diffraction. Nano Letters. 2015;**15**:5630-5634

[20] Wu Y, Islama A, Yang X, Qin C, Liu J, Zhang K, Penga W, Han L. Retarding the crystallization of PbI_2 for highly reproducible planar-structured perovskite solar cells *via* sequential deposition. Energy and Environment Science. 2014;**7**:2934-2938

[21] Jeon YJ, Lee S, Kang R, Kim JE, Yeo JS, Lee SH, Kim SS, Yun JM, Kim DY. Planar heterojunction perovskite solar cells with superior reproducibility. Scientific Reports. 2014;**6953**:1-7

[22] Forouhi A, Bloomer I. Optical dispersion relations for amorphous semiconductors and amorphous dielectrics. Physical Review B. 1986;**34**:7018-7026

[23] Jobin Yvon J. New amorphous dispersion formula. (accessed Oct29, 2015). Available from: http://www. Horiba. Com/fleadmi/New_amorphous_dispersion_formula pdf

[24] Aspnes DE. Optical properties of thin films. Thin Solid Films. 1982;**89**:249-262

[25] Schliiter ICh, Schliiter M. Electronic structure and optical properties of PbI_2. Physical Review B. 1974;**9**:1652-1665

[26] Shirayama M, Kadowaki H, Miyadera T, Sugita T, Kato M, Murata D, Hara S, Murakami T, Chikamatsu M, Fujiwara H. Optical transitions in hybrid perovskite solar cells. Physical Review Applied. 2016;**5**:01402

[27] Lopper P, Stuckellger M, Niesen B, Werner J, Filpie M, Moon SJ, Yum JH, Topic M, Wolf D, Ballif C. Complex refractive index spectra of $CH_3NH_3PbI_3$ perovskite thin films determined by spectroscopic ellipsometry and spectrophotometry. Physical Chemistry Letters. 2015;**6**:66-71

[28] Ishihara T, Takahashi J, Goto T. Optical properties due to electronic transitions in two-dimensional semiconductors $(C_nH_{2n}+1NH_3)_2PbI_4$. Physical Review. 1990;**B42**:11099-11107

[29] Hirasawa M, Ishihara T, Goto T. Exciton features in 0-, 2-, 3-dimensional networks of $[PbI_6]^{4-}$ octahedra. Journal of the Physical Society of Japan. 1994;**63**:3870-3879

[30] Yamanaka T, Masumori K, Ishikawa R, Shirai H. Role of isopropyl alcohol (IPA) in the synthesis of perovskite thin films by two-step method. Journal of Physical Chemistry. 2016;**120**(44):25371-25377

IntechOpen